Desalination and Water Treatment
www.deswater.com

doi: 10.5004/dwt.2020.24825

173 (2020) 213–222
January

Humic acid adsorption behavior and mechanism comparison between biochars and activated carbon

Xiaoju Yan[a], Wei Du[a], Cong Ma[b,*], Shirong Cheng[a], XueYan Li[c]

[a]*College of Hydrology and Water Resources, Hohai University, Nanjing, 210024, China, Tel. +86 13912993906; email: wshyxj@126.com (X.J. Yan), Tel. +86 18705150535; emails: 2087198470@qq.com (W. Du); 270169960@qq.com (S.R. Cheng)*
[b]*State Key Laboratory of Separation Membranes and Membrane Processes, School of Environmental and Chemical Engineering, Tianjin Polytechnic University, Tianjin, 300387, China, Tel. +86 15122382805; email: macong_0805@126.com*
[c]*School of Environmental Science and Engineering, Suzhou University of Science and Technology, Suzhou 215009, China, Tel.+86 13771804391; email: lxyhit@sina.com*

Received 25 August 2018; Accepted 25 August 2019

ABSTRACT

This study aims to compare the adsorption behavior and mechanism of humic acid (HA) on bamboo biochar (BC), helm palm biochar (HP) and activated carbon(AC). Physicochemical properties of absorbents were characterized. The adsorption isotherm models and adsorption kinetic models were analyzed. To characterize the HA before and after adsorption, molecular weight (MW) analysis and three dimensional excitation–emission matrix fluorescence spectroscopy (3D-EEM) analysis were used. The results showed that BC exhibited a better performance than AC and HP for removing HA from both HA solution and natural water. The porous structure distribution, pore volume and polar functional groups of adsorbents were correlated with adsorption capacity. And HA adsorption on adsorbents could be controlled by chemical adsorption.

Keywords: Humic acid (HA); Biochar; Adsorption; Molecular weight (MW)

1. Introduction

Humic acid (HA) is one of the most important fraction of natural organic matter (NOM) and is ubiquitously present in aquatic environments [1]. HA is composed of aromatic and aliphatic structures and functional groups. Their molecular weight (MW) varies from a few hundred to a hundred thousand. The presence of HA in drinking water may cause undesirable color, taste, and odor [2]. Moreover, HA can react with chloride to produce disinfectant by-products such as trihalomethanes that are harmful to human health [3]. Conventional treatment processes such as membrane separation and chemical coagulation are not the best methods to remove HA, as HA tends to foul the membranes, and also the high cost of chemical coagulation [4]. Therefore, it is of great importance to develop effective methods to remove HA in drinking water.

An adsorption process is a simple and universal approach to eliminate organic pollutants in water. Studies about the removal of HA by activated carbon (AC) indicated that HA adsorption to AC is mainly associated with the porous structure, surface chemistry of the adsorbent, and the surface functionality of HA [5]. HA molecules were adsorbed into pores with compatible size in AC [6]. Starek et al. [7] used AC and activated charcoal cloths for HA adsorption and concluded that mesopores and macropores were effective for HA adsorption, but micropores were inaccessible for HA due to size exclusion effect. The adsorption of humic substances requires the material with well-developed mesoporous texture due to large sizes of their molecules [7].

* Corresponding author.

Biochar is a by-product obtained by pyrolyzing biomass at a certain temperature, which is often conducted to gain bio-oil [8]. The specific properties of biochar, including its well-developed porous structure and its enriched surface functional groups, make it possible to be used as proper adsorbent to remove organic pollutants from aqueous solutions [9]. Compared with AC, biochar is cheaper and readily available, because the feedstock of biochar is abundant and low-cost, and the production process of biochar needs less energy than AC [10].

The main objective of this study was to evaluate and compare the HA adsorption performance of biochar and commercial AC, and to observe the possibility of biochar application in drinking water treatment. The characteristics of HA before and after adsorption were elucidated by MW distribution and 3D-EEM analyzing. The physicochemical properties of the biochars and commercial AC were characterized to determine the mechanisms and adsorption characteristics of HA.

2. Materials and experiments

2.1. Materials

All reagents used in this experiment were of analytical grade. HA was purchased from Sigma Chemical Company (America). Natural water treated was collected from the Jinchuan River of Nanjing, southeast of China. The AC was purchased from Chengdu Kelong Chemical Reagent Factory (China), and biochars were pyrolyzed at 600°C for 6 h in the atmosphere of pure nitrogen by the Chinese Academy of Science (China).

2.2. Characterization of adsorbent

The elemental analysis for C, O, H, N of the obtained samples was performed using an Elemental analyzer (Elementar, Vario EL, Germany). The ash content was determined by heating the biochars. The oxygen content was calculated by subtracting the ash, carbon hydrogen, and nitrogen contents from the total mass of the sample. The specific surface areas (SSAs) of the samples were measured by a surface area analyzer (BET, Merck, ASAP20, Germany) with N_2 adsorption. The surface physical morphology was observed using a scanning electron microscope (SEM, Hitachi, S-4800N, Japan). The XRD analysis was performed by a diffractometer (XRD, D/max-2500PC, Rigaku, Japan) with the scan range of 10°–80°. The pH of biochar and AC was determined following the IBI Biochar Standards Version 2.0 using the Test Category A method [30]. Specifically, 0.5 g of adsorbent was mixed with 10 mL of deionized water in a 150 mL Conical flask for a shaking incubating period of 90 min (150 rpm, 30°C). The pH determination was performed in duplicate.

2.3. Characterization of HA

The concentration of HA was measured by UV–vis spectrophotometer (UV-1200, Mpuda, China) in terms of absorbance at 254 nm.

Gel permeation chromatography (GPC, Agilent HPLC 1260 equipped with gel chromatographic column, America) was used to measure the molecular weight of HA solution and Jinchuan river water before and after adsorption by AC and biochars. The system was operated with dimethyl formamide as the eluent at a flow rate of 1 mL/min and calibrated with sodium polystyrene sulfonate standards in the molar mass range from 7.5×10^2 to 2.6×10^6 Da. The column chromatography was performed using a silica gel of 300–400 mesh.

Three-dimensional excitation–emission matrix (3D-EEM) fluorescence spectra of HA solution and Jinchuan river water before and after adsorption by AC and biochars were collected by a fluorescence spectrophotometer (F-7000, Hitachi, Japan), with the scanning emission (Em) spectra from 220 to 580 nm at 5 nm increases by varying the excitation wavelength (Ex) from 220 to 580 nm at 5 nm sampling intervals.

2.4. Batch adsorption experiments

Batch experiments were carried out with the adsorption of HA by BC, HP and AC in aqueous solutions. HA solution and adsorbents were placed in Erlenmeyer flasks (150 mL) in an orbital shaker at 20°C. For adsorption kinetics, each Erlenmeyer flask was filled with a mixture of 0.2 g adsorbent and 100 mL HA solution of 10 mg/L, and agitated for intervals from 15 min to 48 h. The mixture was agitated at 150 rpm. Adsorption isotherm experiments were conducted by filling each Erlenmeyer flask with 0.2 g adsorbent and 100 mL HA solution of six different initial concentrations 2, 5, 10, 20, 30, and 40 mg/L for 48 h to determine the equilibrium concentration. The samples were centrifuged at 3,000 rpm for 5 min before being filtered through 0.45 μm pore size nylon membranes. All experiments (adsorption test; isotherm, and kinetic experiments) were conducted in duplicate. The adsorption capacity q_t (mg/g) was calculated as:

$$q_t = \frac{\left(C_0 - C_t\right)V}{m} \tag{1}$$

where q_t is the adsorption capacity at time t, C_0 and C_t (mg/L) are the initial HA concentration and HA concentration at time t, respectively, V (L) is the volume of solution and m (g) is the dry mass of adsorbent.

2.5. Adsorption isotherm models

The data of adsorption isotherms were fitted with Langmuir, Freundlich, and Temkin models. The Langmuir model, which describes a monolayer adsorption of molecules onto a homogenous adsorbent surface, can be described as Eq. (1):

$$\frac{C_e}{q_e} = \frac{1}{k_L q_m} + \frac{1}{q_m} C_e \tag{2}$$

where q_e (mg/g) is the equilibrium adsorption capacity of the adsorbent; q_m (mg/g) is the maximum adsorption capacity of the adsorbent and k_L (L/mg) is the Langmuir constant related to the energy of adsorption [11]. The isotherm model was expressed in terms of the dimensionless constant separation factor (R_L):

$$R_L = \frac{1}{1 + k_L C_0} \tag{3}$$

where C_0 (mg/L) is the initial adsorbate concentration. Values of $R_L = 0$, $0 < R_L < 1$, $R_L = 1$ and $R_L > 1$ are indicative of irreversible, favorable, linear and unfavorable adsorption process, respectively [12].

The Freundlich model, which describes a multilayer coverage of adsorbed molecules onto heterogeneous surfaces, assuming that adsorbent surface sites have a spectrum of different binding energies, can be expressed as Eq. (4):

$$q_e = k_F C_e^{\frac{1}{n}} \tag{4}$$

where q_e (mg/g) is the equilibrium adsorption capacity of the adsorbent; k_F ([(mg g^{-1})·$mg^{1/n}$]) is the Freundlich affinity coefficient, C_e (mg/L) is the equilibrium solution concentration after adsorption and $1/n$ is the Freundlich exponential coefficient. Value of $1/n$ close to zero indicates more surface heterogeneity, below one demonstrates Langmuir isotherm, whereas above one indicates cooperative adsorption [13].

The Temkin model, which is considered the effects of indirect adsorbent/adsorbate interactions on adsorption isotherms, assumes that the heat of adsorption of all the molecules in the layer decreases linearly with coverage due to adsorbent/adsorbate interactions, expressed as Eq. (5):

$$q_e = \frac{RT}{b_T} \ln\left(A_T C_e\right) \tag{5}$$

where R (8.314 J/(mol K)) is the universal gas constant, T (K) represents absolute temperature, b_T (J/mol) is the constant related to heat of adsorption and A_T (1/mg) is the equilibrium binding constant.

2.6. Adsorption kinetic models

Three kinetic models, the pseudo-first order, pseudo-second order, and intra-particle diffusion models were used to fit the experimental data. Pseudo-first order kinetic model in linear form can be expressed as Eq. (6):

$$\ln\left(q_e - q_t\right) = \ln q_e - k_1 t \tag{6}$$

The pseudo-second order linear equation is as follows:

$$\frac{t}{q_t} = \frac{1}{k_2 q_e^2} + \frac{t}{q_e} \tag{7}$$

$$h = k_2 q_e^2 \tag{8}$$

where q_e (mg/g) is the adsorption capacity at equilibrium. k_1 (1/h) and k_2 (g/mg h) are the rate constants of pseudo-first and pseudo-second order kinetics.

The intra-particle diffusion model [14] has been mainly used to predict the role of diffusion, which can be described as:

$$q_t = k_p t^{0.5} + C \tag{9}$$

where k_p (mg/g $h^{-0.5}$) is the intra-particle diffusion rate constant.

3. Results and discussion

3.1. Adsorption capacity and characterization of biochar

The adsorption capacity values at initial concentrations of 10 mg/L HA are shown in Table 1. Adsorption capacities of BC are higher than those of AC and HP. Their adsorption performance was greatly affected by the elemental composition, structural characteristics, and surface properties of adsorbents.

The detailed composition and other physicochemical properties of the adsorbents are listed in Table 1. The H/C ratio of HP (0.019), BC (0.018), and AC (0.018) indicating that the aromaticity of the three adsorbents is similar [15–17]. The O/C ratio of these three adsorbents is HP < AC < BC (0.051 < 0.075 < 0.095), suggesting that HP and AC are less hydrophobic than BC [18,19]. The polarity index [(O + N)/C] is HP < AC < BC (0.061 < 0.081 < 0.095) suggests that BC has higher portion of O-containing (polar) functional groups [20,21]. The higher polarity of biochar enhanced the adsorption affinity toward polar compounds due to delocalization of the aromatic π-cloud [19]. Polarizability may lead to induced electrostatic interactions (π–π interaction, π-stacking, and London dispersion forces) as well as hydrophobic interactions between compounds (π acceptors) and adsorbents having aromatic benzene rings (π donors) [22].

The presence of ash can concentrate oxygenated polar functional groups on the outer surface of biochar [23]. The ash ratio of three adsorbents is HP < AC < BC (6.89% < 8.98% < 10.32%), suggesting that BC has more polar functional groups on the surface, which is the same conclusion in polarizability analysis. From elemental composition analysis, adsorption capacity of BC is higher than that of AC and HP, maybe due to the higher polarizability of BC.

N_2 adsorption experiments were conducted to determine the porous structure of AC and biochar (Table 2). The SSAs of BC biochars are slightly lower than those of AC, the pore volume of BC biochars are much higher than AC and

Table 1
Physical and chemical properties of the adsorbents

Adsorbent	q_e (mg g^{-1})	C%	H%	O%	N%	H/C	O/C	(N + O)/C	Ash (%)	pH
BC	2.421	80.61	1.42	7.65	0	0.018	0.095	0.095	10.32	7.59
HP	1.105	84.29	1.61	4.32	0.8	0.019	0.051	0.061	8.98	8.56
AC	1.108	84.7	1.51	6.32	0.58	0.018	0.075	0.081	6.89	9.37

Table 2
BET results of adsorbents

Adsorbent	A_{BET}(m²/g)	D_p(nm)	PV (cm³/g)
	261.2	3.17	0.099
HP	125.9	3.05	0.020
AC	329.0	3.10	0.027

HP biochar. However, adsorption capacity of BC biochars is higher than AC and HP biochars, which is due to that the pore size and pore volume are more important than the adsorption capacity of large molecules on the SSA in adsorption capacity [24].

According to the BJH adsorption pore size distribution shown in Fig. 1. The BC, AC, and HP have an average maximum volume at pore size of 3.17, 3.10 and 3.05 nm, separately. They are in the small mesoporous range. The presence of mesopores (2–50 nm) is crucial in the adsorption process of HA.

AC and HP biochars have pore size of 1–5 nm. Compared with AC and HP biochars, BC biochars have a broader pore size distribution. The adsorbents with large pores, broad pore size distribution and large pore volume were better in HA adsorption [25]. Therefore, adsorption capacity of BC biochars is higher than that of AC and HP biochars.

The morphology of adsorbents is shown in Fig. 2. It can be seen that AC and HP biochar images showed a more amorphous and fewer surface pores structure compared with BC. According to a previous study [26], crystalline structures results of dehydration of cellulose showed that AC and HP biochars might have lower content of cellulose, corresponding to their more amorphous structure. BC biochars had a rough surface, regular shape, and many holes, which could promote the adsorption of HA due to the bigger surface area of biochar, and the larger number of porous sites on its surface [27,28].

The XRD patterns of AC, HP, and BC are shown in Fig. 3. Two main peaks are present for all three adsorbents, including a broad diffraction peak (2θ = 23°~26°) attributed to disordered structures in chars including amorphous carbon and aliphatic side chains, as well as a weak broad diffraction peak (2θ = 40°~50°) resulting from the graphitic structure [29]. Moreover, the XRD results indicate that the HP and BC biochars contain crystal phase compositions. The major peaks of the BC biochar were observed from Fig. 3b, peak A appeared at 29°, 36.5°, 39.5°, 43°, 47°, 56.5°, 61.2°, corresponding to $CaCO_3$, peaks B appeared at 36.5°, 56.5°, 61.2° were ascribed to $CaSi_2$. The major peaks of the HP biochar were observed from Fig. 3c, peak C appeared at 20.54°, 29.12° were ascribed to SiS_2, peaks D appeared at 26.32°, 49.78°, 59.66°, 67.92° were ascribed to SiO_2. The crystals on biochar surface are produced during pyrolysis at high temperatures and the greater prevalence of these peaks is consistent with the higher percentage of ash in the biochar, which enhanced adsorption [26].

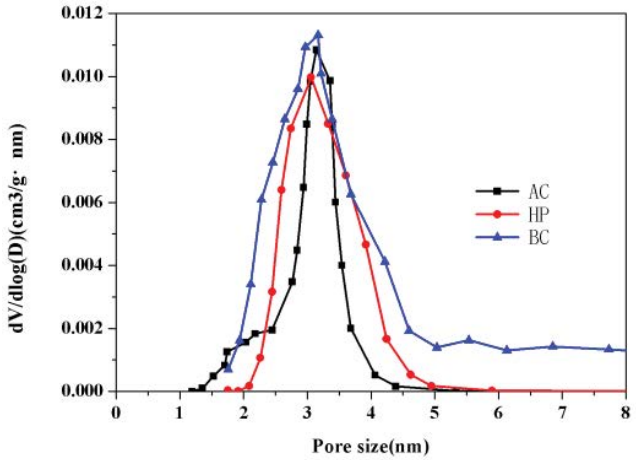

Fig. 1. Average pore size distribution of adsorbents.

Fig. 4 presents the FTIR spectra of adsorbents, where a large number of functional groups can be observed. The strong and broad peak around 3,438 cm^{-1} indicates the existence of –OH group [30]. The band at 2,353 cm^{-1} is assigned to functional groups of C=O, this is due to the bending vibration of C=O on aromatic rings on carbon surface [29]. The sharp peak at 1,631 cm^{-1} is related to the C=O stretching vibration [26]. The peak at 1,438 cm^{-1}indicates the presence of aromatic C=C stretching [26]. Characteristic peaks for biochar occurred at indicative of C–O stretching and the peak at approximately 533 cm^{-1} can be ascribed to the inorganic oxide [31]. Compared with AC, more O-containing (polar) functional groups are present on the surfaces of biochars, which is consistent with the results of the elemental analysis. More functional groups indicate that it is easier to form chemical bonds with organic matter and thus increase the amount of adsorption.

3.2. Adsorption kinetics

Three different kinetic models were applied to determine the rate determining step for HA adsorption. The kinetic experimental data were characterized by the initial rapid reaction during the first 4 h. The kinetic model parameters are listed in Table 3. The fitting curve is shown in Fig. 5. Among the three models tested, the pseudo-second order fits the experimental data better with R^2 of 0.977, 0.981, and 0.975 for BC, HP, and AC, separately, indicating that HA adsorption onto adsorbents could be controlled by chemical adsorption, and that the adsorption capacity is proportional to the number of active sites of adsorbents [32].

According to intra-particle model, the fitting lines do not pass through the origin ($C = 0$) means that the intra-particle diffusion is not the rate controlling step. All adsorbents show intra-particle model parameter, $C > 0$, which suggested that mass transfer of HA across the boundary layer was rate determining.

3.3. Adsorption isotherms

Three isotherm models including Langmuir, Freundlich, and Temkin were fitted. The results are shown in Fig. 6. It can be seen that the sorption isotherms for BC and AC were quite well simulated by the three isotherm models with $R^2 > 0.95$, indicating that not a unique mechanism of sorption can be individuated in this case [15].

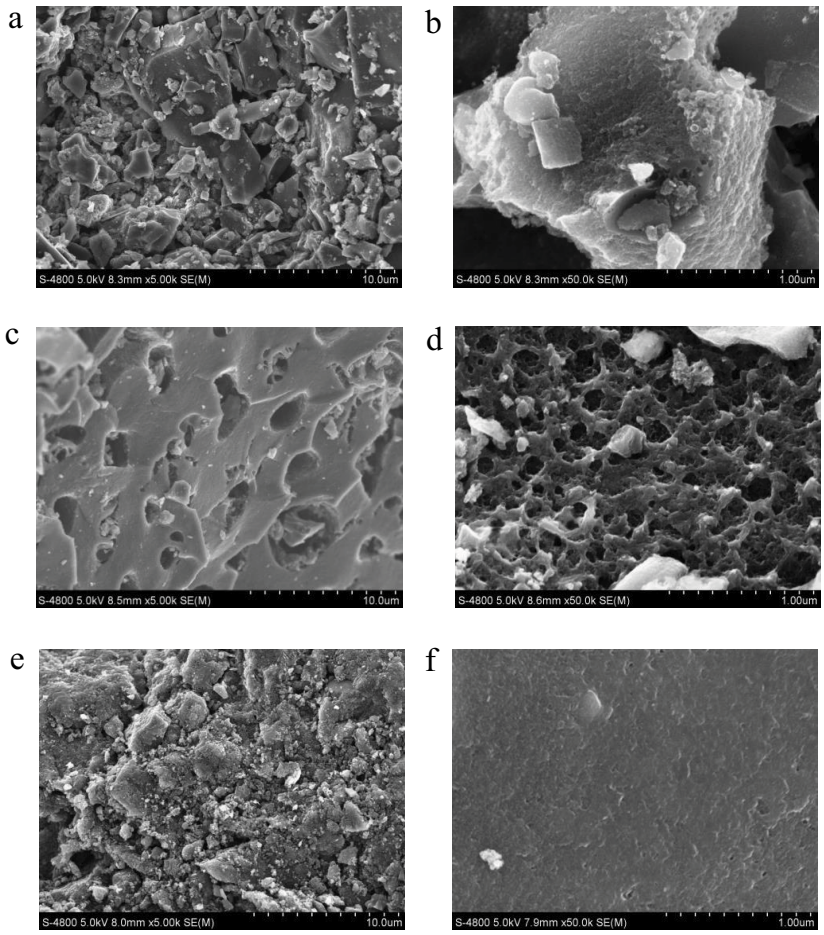

Fig. 2. SEM spectra of AC (a, b), BC (c, d), and HP (e, f).

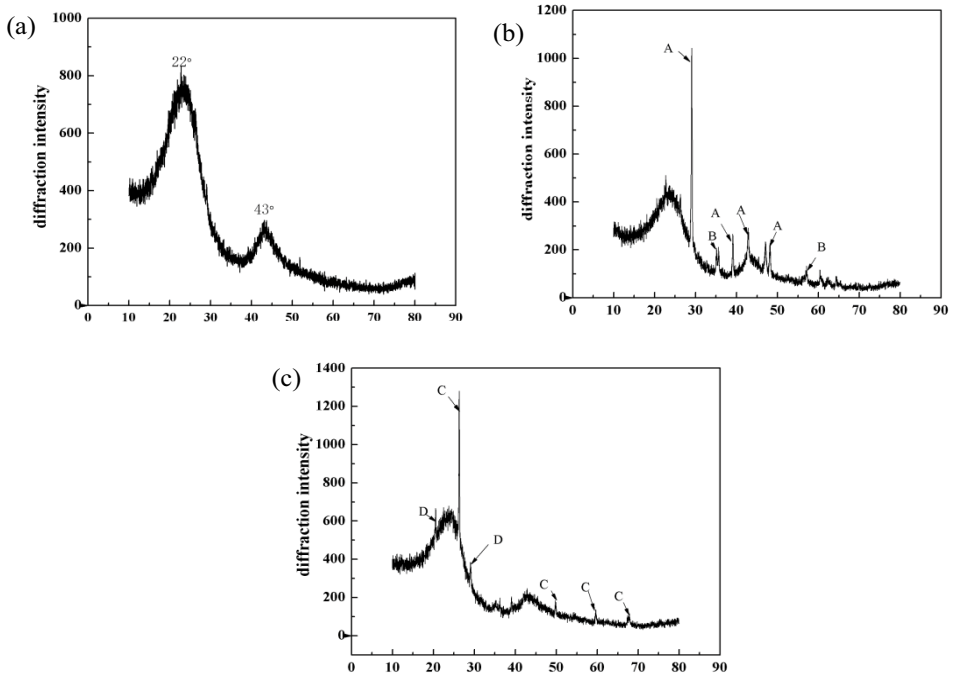

Fig. 3. XRD spectrum of adsorbents: (a) AC; (b) BC; (c) HP.

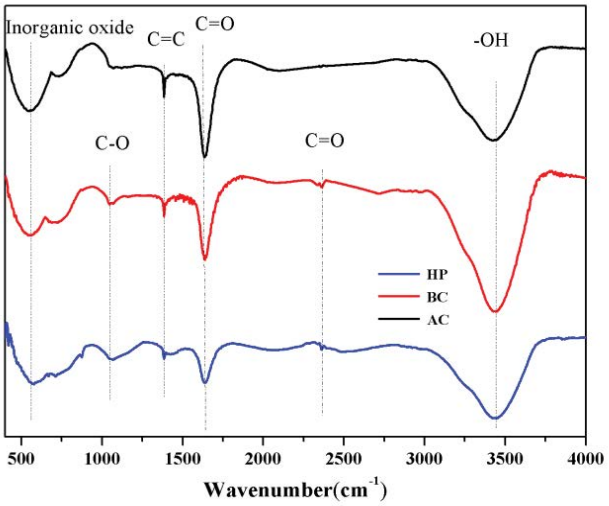

Fig. 4. Fourier transform infrared spectroscopy (FTIR) of adsorbents.

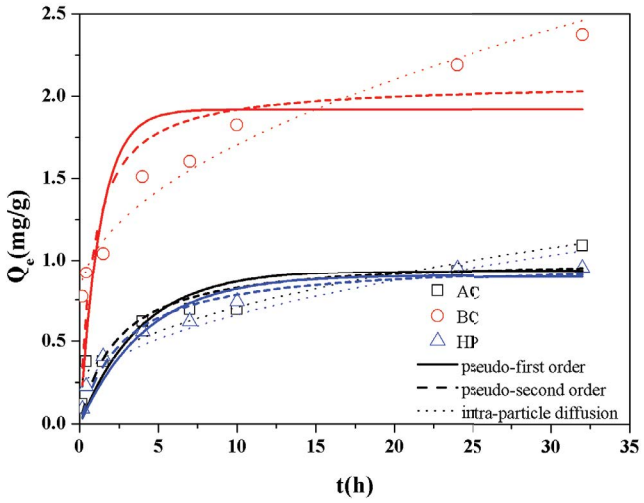

Fig. 5. Adsorption kinetics of HA onto adsorbents.

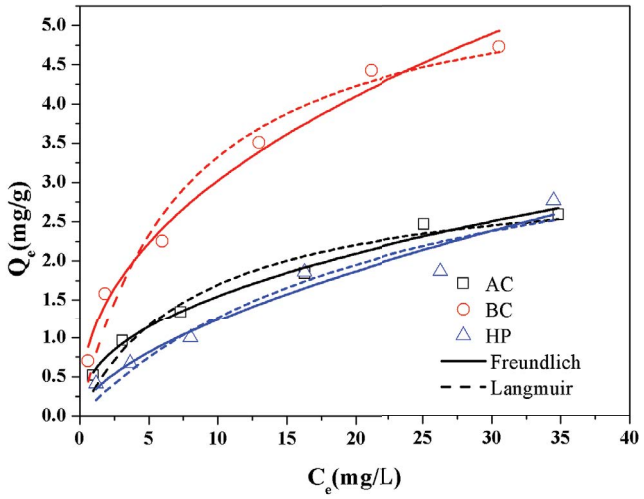

Fig. 6. Adsorption isotherms of HA by adsorbents.

Table 3
Kinetic simulation results

Adsorbent	Pseudo-first order				Pseudo-second order				Intra-particle diffusion			
	q_e (exp)/(mg g^{-1})	q_e (cal)/(mg g^{-1})	k_1/L h^{-1}	R^2	q_e (exp)/(mg g^{-1})	q_e (cal)/(mg g^{-1})	k_2/g·(mg h)$^{-1}$	h/[mg·(g h)$^{-1}$]	R^2	k_p/[mg·(g h$^{0.5}$)$^{-1}$]	C	R^2
BC	2.432	3.250	0.217	0.960	2.421	2.421	0.183	1.077	0.977	0.295	0.730	0.969
HP	0.952	0.519	0.285	0.950	1.105	1.014	0.375	0.457	0.981	0.183	0.122	0.950
AC	1.088	0.525	0.160	0.935	1.108	1.108	0.310	0.380	0.975	0.159	0.204	0.936

The maximum adsorption capacity values obtained from the Langmuir model indicate that the BC biochar has the best performances. The high q_m maybe due to higher pore volume and more broad pore size distribution of BC than that of AC and HP biochar. And also, BC has more polar functional groups on the surface. The separation factor R_L value implies that the adsorption process is favorable for three adsorbents tested (R_L 0.29–0.59).

All the adsorbents were better described by Freundlich which indicates ore surface heterogeneity. Table 4 shows that 1/*n* of the three adsorbents were less than 1 (0.45–0.55), also suggesting that the adsorption process is favorable.

Table 5 indicates the comparison with literature regarding the adsorption capacities and adsorption kinetics.

3.4. Characterization of NOM before and after adsorption

To characterize the NOM before and after adsorption, the adsorption experiments were carried out using HA solution and Jinchuan river water. The MW distribution and 3d-EEM spectroscopy of water sample were analyzed. An Erlenmeyer flask was filled with a mixture of 0.2 g adsorbent and 100 mL HA solution (20 mg/L) or Jinchuan river water, shaken at 20 C for 48 h.

Fig. 7 shows the MW distribution of HA solution and Jinchuan river water before and after adsorption on three adsorbents. Fig. 7a indicates the peaks at 5.18 and 6.75 min correlated with the HA MW above 57,000 and 1,800 Da, respectively. Fig. 7b indicates the peaks at 7.02 and 7.29 min

Table 4
Adsorption isotherms

Model		Langmuir				Freundlich			Temkin		
		q_m/(mg g^{-1})	k_L/L mg^{-1}	R_L	R^2	k_F/[(mg/g)(mg/L)$^{-1/n}$]	1/*n*	R^2	b_T/(J mol^{-1})	A_T/(mg^{-1})	R^2
HA	BC	5.1546	0.2495	0.3241	0.9584	1.0040	0.4785	0.9810	2,334.5	2.52	0.9593
	HP	3.4083	0.0694	0.2861	0.8486	0.3499	0.5531	0.9743	3,790.9	1.03	0.8645
	AC	2.8145	0.2085	0.5903	0.9526	1.8331	0.4501	0.9939	4,126.0	1.88	0.9550

Table 5
Comparison of the adsorption capacity of adsorbents for HA in this study and other adsorbents in literature

Adsorbent	pH	q_m[a]/(mg/g)	k_F[b]/[(mg/g)(mg/L)$^{-1/n}$]	q_e[c]/(mg/g)	Reference
Granular activated carbon	7	–	1.09	16	[33]
Activated biochar	7	–	1.39	9.04	[34]
Powdered activated carbon	7	–	1.06	–	
Raw bentonite	6	26	–	15	[35]
SMC-800-0.25	7	540	15.9	27.3	[24,25]
AC	7	236	9.64	20.6	
Bamboo biochar	6.5	5.1546	1.004	2.421	This study
Helm palm biochar	6.5	3.4083	0.3499	1.105	This study
Activated carbon	6.5	2.8145	1.8331	1.108	This study

[a]q_m is the maximum adsorptive capacity of the adsorbent in Langmuir model.
[b]k_F is Freundlich constant related to adsorption capacity.
[c]q_e is the amount of adsorbate adsorbed at equilibrium.

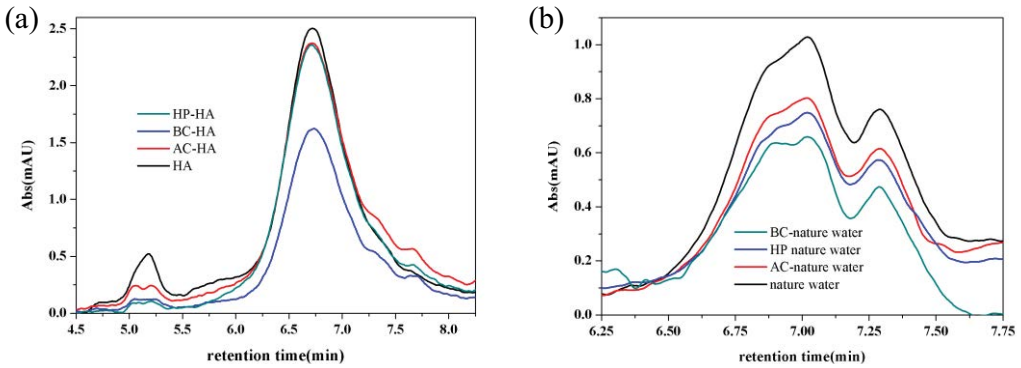

Fig. 7. Removal rate of humic acids of different MW: (a) HA solution and (b) Jinchuan river.

correlated with the NOM MW of 900 and 500 Da. After adsorption, the entire chromatogram of BC biochars is lower than that of AC and HP biochars, which is due to that BC biochars with large pores and a broad pore size distribution can adsorb more NOM molecules [25].

It is notable from the EEM spectra of HA solution (Fig. 8) that there is one major peak of HA solution identified at excitation/emission wavelengths Ex/Em = 220–290/420–460 nm (Peak E), which represents HA. Peak E shows an evident change after adsorption by three adsorbents, while the peak height of BC is lowest, which shows the lowest concentration of HA. This is consistent with adsorption capacity of adsorbent.

Fig. 9 shows that four peaks were identified from EEM fluorescence spectra. The first main peak was identified at excitation/emission wavelengths (Ex/Em) of 220–290/320–360 nm (Peak A), while the second main peak was identified at Ex/Em of 200–240/320–360 nm (Peak B). The two peaks have been described as protein-like peaks, in which the fluorescence is associated with the aromatic amino acid tryptophan. Another two peaks were located around Ex/Em = 220–240/280–320 nm (Peak C) and Ex/Em = 220–290/280–320 nm (Peak D), which represent tyrosine [36,37]. Fig. 9 illustrates that there are mainly protein-like substances in Jinchuan river. After adsorption on BC biochars, peak A and peak C completely disappeared, and there is an obvious decrease in the peak heights of peaks B and D. Moreover, after adsorption on AC and HP biochars, peak heights of peaks A to D decreased more than those of Jinchuan river, but still higher than those after BC biochars adsorption. It should be concluded that the protein-like substances in natural water are almost removed by adsorption, and BC biochars show a better performance.

3.5. Influence of the pH

The effect of pH on adsorption of HA onto adsorbents was investigated. Fig. 10 indicates that the HA adsorption decreases with the pH value, which is because that the charge of HA molecules changes with pH. The success dissociation of carboxylic and phenolic hydroxyl group enhance the negative charge of HA molecules and cause electrostatic repulsion with the hydrophobic and more negatively charged carbon surface, hence induce the lower adsorption. As the pH decreases, carboxyl and phenolic hydroxyl groups of HA are protonated. Less negative charge on carbon surface, decreases electrostatic repulsion, and increases the hydrophobic interactions; hence, increases the adsorption [25]. Meanwhile, HA molecules may become smaller in size due to the tendency to coil at low pH value, which is also contributing to the higher adsorption capacity [33].

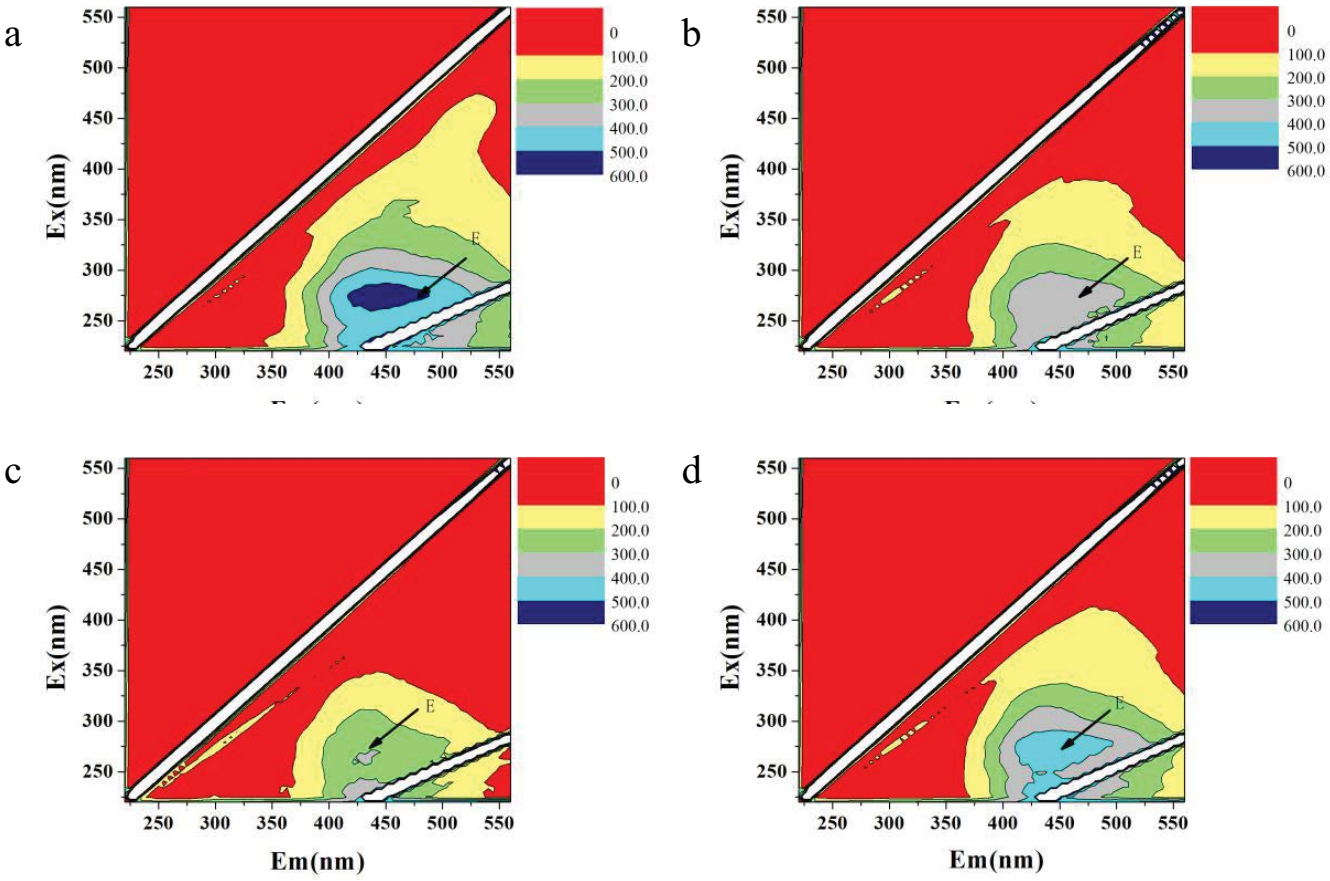

Fig. 8. EEM spectra of humic acid (a) before adsorption; (b) after adsorption by AC; (c) after adsorption by BC; (d) after adsorption by HP.

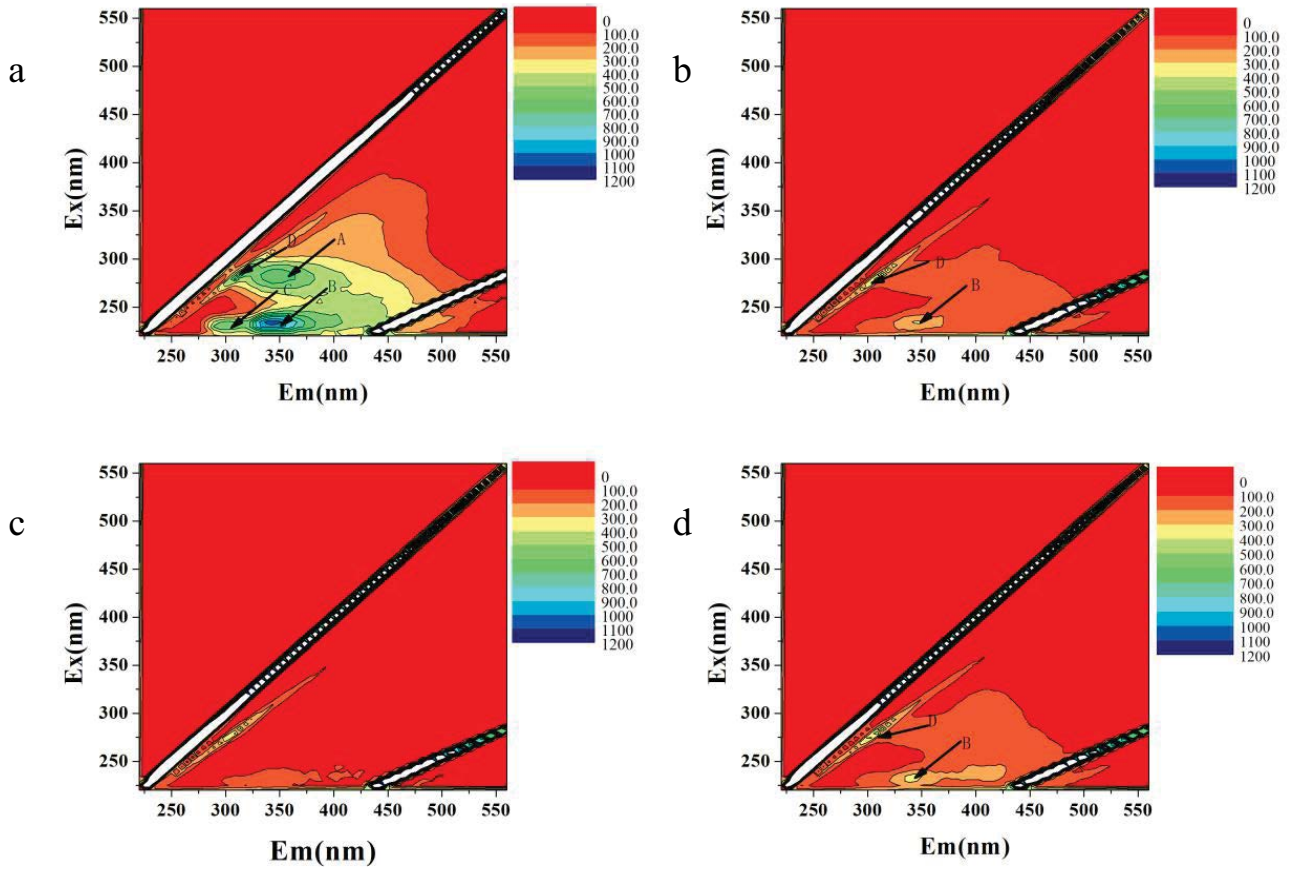

Fig. 9. EEM spectra of Jinchuan river (a) before adsorption; (b) after adsorption by AC; (c) after adsorption by BC; (d) after adsorption by HP.

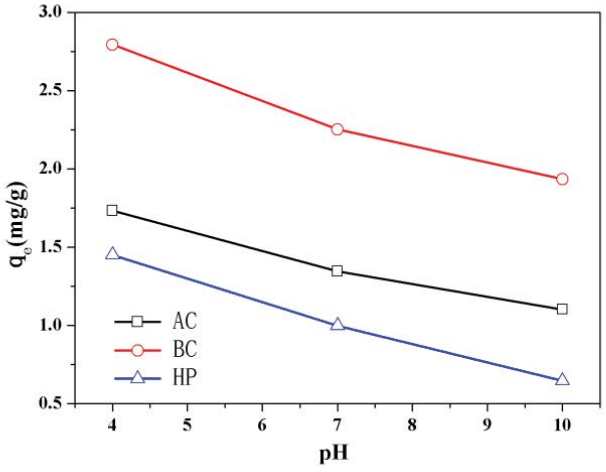

Fig. 10. Influence of initial pH on the adsorption capacity.

4. Conclusions

In this study, adsorption behavior and mechanism comparison of HA on biochars and commercial activated carbon were studied. The results showed that equilibrium adsorption capacity q_e of humic acid of BC was much larger than that of AC and HP. The better performance of BC was due to its higher pore volume and more broad pore size distribution than AC and HP biochar. Moreover, BC with more polar functional groups on the surface made it easier to combine with HA. Therefore, BC was an appropriate absorbent in drinking water treatment. The pseudo-second-order kinetics fit the experimental data better, indicating that HA adsorption on adsorbents can be controlled by a chemical adsorption. All the adsorbents were better described by Freundlich isotherm, which showed more surface heterogeneity. Moreover, pH can affect the structure of HA molecules and the interaction force between adsorbent and HA molecules, thus affecting the adsorption capacity.

Acknowledgments

This work is supported by the Fundamental Research Funds for the Central Universities (2017B10414), the National Science Foundation of China (51208172, 51508383 and 51508384) and the Natural Science Foundation of Tianjin Province (18JCQNJC09000).

References

[1] X. Qin, F. Liu, G. Wang, G. Huang, Adsorption of humic acid from aqueous solution by hematite: effects of pH and ionic strength, Environ. Earth Sci., 73 (2015) 4011–4017.

[2] Q. Tao, Z. Xu, J. Wang, F. Liu, H. Wan, S. Zheng, Adsorption of humic acid to aminopropyl functionalized SBA-15, Microporous Mesoporous Mater., 131 (2010) 177–185.
[3] A. Kerc, M. Bekbolet, A.M. Saatci, Effect of partial oxidation by ozonation on the photocatalytic degradation of humic acids, Int. J. Photoenergy, 5 (2003) 75–80.
[4] E. Lorenc-Grabowska, G. Gryglewicz, Adsorption of lignite-derived humic acids on coal-based mesoporous activated carbons, J. Colloid Interface Sci., 284 (2005) 416–423.
[5] S. Han, S. Kim, H. Lim, W. Choi, H. Park, J. Yoon, T. Hyeon, New nanoporous carbon materials with high adsorption capacity and rapid adsorption kinetics for removing humic acids, Microporous Mesoporous Mater., 58 (2003) 131–135.
[6] H. Tamai, T. Kakii, Y. Hirota, T. Kumamoto, H. Yasuda, Synthesis of extremely large mesoporous activated carbon and its unique adsorption for giant molecules, Chem. Mater., 8 (1996) 454–462.
[7] J. Stárek, A. Zukal, J. Rathouský, Comparison of the adsorption of humic acids from aqueous solutions on active carbon and activated charcoal cloths, Carbon, 32 (1994) 207–211.
[8] D. Özçimen, A. Ersoy-Meriçboyu, Characterization of biochar and bio-oil samples obtained from carbonization of various biomass materials, Renew. Energy, 35 (2010) 1319–1324.
[9] W. Chen, R. Parette, J. Zou, F.S. Cannon, B.A. Dempsey, Arsenic removal by iron-modified activated carbon, Water Res., 41 (2007) 1851–1858.
[10] M. Ahmad, S.S. Lee, X. Dou, D. Mohan, J.K. Sung, J.E. Yang, Y.S. Ok, Effects of pyrolysis temperature on soybean stover- and peanut shell-derived biochar properties and TCE adsorption in water, Bioresour. Technol., 118 (2012) 536–544.
[11] S. Chatterjee, S.H. Woo, The removal of nitrate from aqueous solutions by chitosan hydrogel beads, J. Hazard. Mater., 164 (2009) 1012–1018.
[12] M.T. Yagub, T.K. Sen, S. Afroze, H.M. Ang, Dye and its removal from aqueous solution by adsorption: a review, Adv. Colloid Interface, 209 (2014) 172–184.
[13] G.O. El-Sayed, Removal of methylene blue and crystal violet from aqueous solutions by palm kernel fiber, Desalination, 272 (2011) 225–232.
[14] S.B. Abdul Hamid, Z.Z. Chowdhury, S.M. Zain, Base catalytic approach: a promising technique for the activation of biochar for equilibrium sorption studies of Copper, Cu(II) ions in single solute system, Materials, 7 (2014) 2815–2832.
[15] B. de Caprariis, P. De Filippis, A.D. Hernandez, E. Petrucci, A. Petrullo, M. Scarsella, M. Turchi, Pyrolysis wastewater treatment by adsorption on biochars produced by poplar biomass, J. Environ. Manage., 197 (2017) 231–238.
[16] P. Peng, Y.H. Lang, X.M. Wang, Adsorption behavior and mechanism of pentachlorophenol on reed biochars: pH effect, pyrolysis temperature, hydrochloric acid treatment and isotherms, Ecol. Eng., 90 (2016) 225–233.
[17] S. Yi, B. Gao, Y. Sun, J. Wu, X. Shi, B. Wu, X. Hu, Removal of levofloxacin from aqueous solution using rice-husk and wood-chip biochars, Chemosphere, 150 (2016) 694–701.
[18] M.I. Al-Wabel, A. Al-Omran, A.H. El-Naggar, M. Nadeem, A.R.A. Usman, Pyrolysis temperature induced changes in characteristics and chemical composition of biochar produced from conocarpus wastes, Bioresour. Technol., 131 (2013) 374–379.
[19] E. Kim, C. Jung, J. Han, N. Her, C.M. Park, M. Jang, A. Son, Y. Yoon, Sorptive removal of selected emerging contaminants using biochar in aqueous solution, J. Ind. Eng. Chem., 36 (2016) 364–371.
[20] W. Ding, X. Dong, I.M. Ime, B. Gao, L.Q. Ma, Pyrolytic temperatures impact lead sorption mechanisms by bagasse biochars, Chemosphere, 105 (2014) 68–74.
[21] G. Zhang, Q. Zhang, K. Sun, X. Liu, W. Zheng, Y. Zhao, Sorption of simazine to corn straw biochars prepared at different pyrolytic temperatures, Environ. Pollut., 159 (2011) 2594–2601.
[22] C.R. Martinez, B.L. Iverson, Rethinking the term "pi-stacking", Chem. Sci., 3 (2012) 2191–2201.
[23] K. Sun, M. Kang, Z. Zhang, J. Jin, Z. Wang, Z. Pan, D. Xu, F. Wu, B. Xing, Impact of deashing treatment on biochar structural properties and potential sorption mechanisms of phenanthrene, Environ. Sci. Technol., 47 (2013) 11473–11481.
[24] W. Libbrecht, A. Verberckmoes, J.W. Thybaut, P. Van Der Voort, J. De Clercq, Soft templated mesoporous carbons: tuning the porosity for the adsorption of large organic pollutants, Carbon, 116 (2017) 528–546.
[25] W. Libbrecht, A. Verberckmoes, J.W. Thybaut, P. Van Der Voort, J. De Clercq, Tunable large pore mesoporous carbons for the enhanced adsorption of humic acid, Langmuir, 33 (2017) 6769–6777.
[26] M. Keiluweit, P.S. Nico, M. Johnson, and M. Kleber, Dynamic molecular structure of plant biomass-derived black carbon (biochar), Environ. Sci. Technol., 44 (2010) 1247–1253.
[27] F. Ma, B. Zhao, J. Diao, Adsorption of cadmium by biochar produced from pyrolysis of corn stalk in aqueous solution, Water Sci. Technol., 74 (2016) 1335–1345.
[28] Y. Yao, Y. Zhang, B. Gao, R. Chen, F. Wu, Removal of sulfamethoxazole (SMX) and sulfapyridine (SPY) from aqueous solutions by biochars derived from anaerobically digested bagasse, Environ. Sci. Pollut. Res., 25 (2018) 25659–25667.
[29] N. Liu, M. Zhu, H. Wang, H. Ma, Adsorption characteristics of Direct Red 23 from aqueous solution by biochar, J. Mol. Liq., 223 (2016) 335–342.
[30] D.D. Sewu, P. Boakye, S.H. Woo, Highly efficient adsorption of cationic dye by biochar produced with Korean cabbage waste, Bioresour. Technol., 224 (2017) 206–213.
[31] B. Chen, Z. Chen, S. Lv, A novel magnetic biochar efficiently sorbs organic pollutants and phosphate, Bioresour. Technol., 102 (2011) 716–723.
[32] A.S. Franca, L.S. Oliveira, M.E. Ferreira, Kinetics and equilibrium studies of methylene blue adsorption by spent coffee grounds, Desalination, 249 (2009) 267–272.
[33] S. Maghsoodloo, B. Noroozi, A.K. Haghi, G.A. Sorial, Consequence of chitosan treating on the adsorption of humic acid by granular activated carbon, J. Hazard. Mater., 191 (2011) 380–387.
[34] C. Jung, N. Phal, J. Oh, K.H. Chu, M. Jang, Y. Yoon, Removal of humic and tannic acids by adsorption-coagulation combined systems with activated biochar, J. Hazard. Mater., 300 (2015) 808–814.
[35] M. Salman, B. El-Eswed, F. Khalili, Adsorption of humic acid on bentonite, Appl. Clay Sci., 38 (2007) 51–56.
[36] Z. Wang, M. Gao, S. Wang, Y. Xin, D. Ma, Z. She, Z. Wang, Q. Chang, Y. Ren, Effect of hexavalent chromium on extracellular polymeric substances of granular sludge from an aerobic granular sequencing batch reactor, Chem. Eng. J., 251 (2014) 165–174.
[37] L.L. Wei, K. Wang, Q.L. Zhao, J.Q. Jiang, X.J. Kong, D.J. Lee, Fractional, biodegradable and spectral characteristics of extracted and fractionated sludge extracellular polymeric substances, Water Res., 46 (2012) 4387–4396.